From Tunneling to Hopping: A Comprehensive Investigation of Charge Transport Mechanism in Molecular Junctions Based on Oligo(*p*-phenylene ethynylene)s

Qi Lu,[†,‡] Ke Liu,[†] Hongming Zhang,[†] Zhibo Du,[†] Xianhong Wang,[†,*] and Fosong Wang[†]

[†]State Key Laboratory of Polymer Physics and Chemistry, Changchun Institute of Applied Chemistry, Chinese Academy of Sciences, Changchun 130022, People's Republic of China, and [‡]Graduate School of the Chinese Academy of Sciences, Beijing 100039, People's Republic of China

ABSTRACT The charge transport mechanism of oligo(*p*-phenylene ethynylene)s with lengths ranging from 0.98 to 5.11 nm was investigated using modified scanning tunneling microscopy break junction and conducting probe atomic force microscopy methods. The methods were based on observing the length dependence of molecular resistance at single molecule level and the current−voltage characteristics in a wide length distribution. An intrinsic transition from tunneling to hopping charge transport mechanism was observed near 2.75 nm. A new transitional zone was observed in the long length molecular wires compared to short ones. This was not a simple transition between direct tunneling and field emission, which may provide new insights into transport mechanism investigations. Theoretical calculations provided an essential explanation for these phenomena in terms of molecular electronic structures.

KEYWORDS: oligo(*p*-phenylene ethynylene)s · charge transport mechanism · tunneling conduction · hopping conduction · scanning tunneling microscopy · conducting probe atomic force microscopy · single molecular resistance

Since its establishment in 1974, molecular electronics has become an interdisciplinary research topic that has the overall aim of constructing and implementing the nanoscale circuits based on single molecular devices.[1−3] Any reasonable design for more efficient molecular devices hinges on a fundamental and comprehensive understanding of charge transport mechanisms in molecular junctions.[4] As predicted theoretically, and proved by many experiments in donor−bridge−acceptor (D−B−A) systems, nonresonant tunneling transport predominates in short molecular wires where molecular resistance varies exponentially with length. In long molecular wires, this is replaced by hopping conduction wherever the resistance has a weak length dependence.[5−8] Although D−B−A investigations provide valuable information on the charge transport characteristics of conjugated bridges involving both transport regimes, it is necessary to expand correlated experiments to molecular junctions (*i.e.*, directly wiring molecules between two metal electrodes) since uncertain effects of donor and acceptor exist on the intrinsic conduction of a conjugated bridge.[9]

On the basis of the sandwiched junction methods, a variety of test beds for direct current−voltage (*I*−*V*) measurement have been disclosed, which include mechanical break junctions,[10,11] nanopores,[2] cross-wire junctions,[12] mercury-drop electrodes,[13] scanning tunneling microscopy (STM),[14−18] and conducting probe atomic force microscopy (CP-AFM),[19−21] *etc.* Recently, using CP-AFM combined with controlled aryl imine addition chemistry, Frisbie and co-workers were able to observe the conduction mechanism transition from tunneling to hopping that occurred in a metal−molecule−metal junction.[22] This factually elucidated the role of molecular length and bond architecture on molecular resistance and opened opportunities for further understanding the transport properties of molecular wires from a new viewpoint.

As one of the most important types of molecular wires, oligo(*p*-phenylene ethynylene)s (OPE) and their derivates, also called by the joint name "Tour Wires", have been utilized extensively in a large number of research fields in molecular electronics.[23−25] These wires carry out many favorable electrical functions including rectification, negative differential resistance (NDR),[26] data storage, and molecular switching,[27−29] *etc.* However, few studies

*Address correspondence to xhwang@ciac.jl.cn.

Received for review September 17, 2009 and accepted November 5, 2009.

Published online November 16, 2009.
10.1021/nn9012687

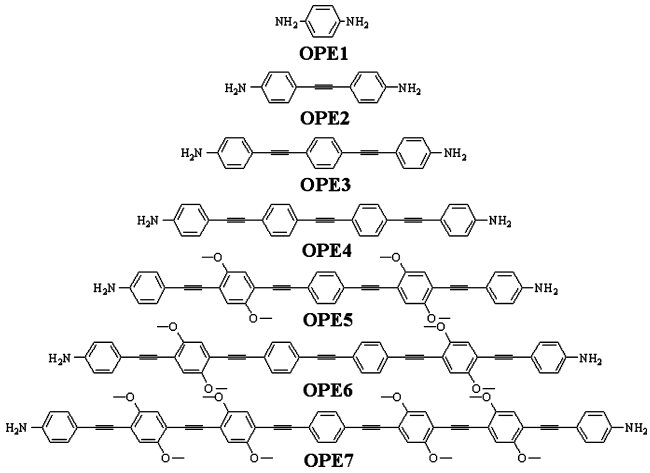

Scheme 1. Structures of seven amine-terminated OPE molecular wires studied in this work.

have yet addressed the charge transport mechanism involving hopping conduction for an OPE system, especially based on molecular junctions. The present paper is therefore focused on three issues: first is to determine the inflection length of OPE system, second is to obtain detailed information of charge transport in both conduction regimes, and the last is to explain all of the phenomena *via* a theoretical calculation approach.

To this end, seven OPE molecular wires (Scheme 1) with different lengths have been used to fabricate molecular junctions. Considering that the variability of observed molecular resistance for diamine molecule−Au junctions is much less than that for dithiol−Au junctions,[30] amine groups were used as linking groups. To enhance the solubility of long OPE molecules, methoxy groups were incorporated, as these would neither prevent the molecules from being anchored with Au nor influence their resistance value.[31] Electronic decay constant, single molecular resistance, and current−voltage characteristics were obtained by STM break junction and CP-AFM measurements. The correlation between charge transport mechanism and molecular electronic structure is intensively discussed.

RESULTS AND DISCUSSION

CV and XPS Measurements for SAMs of OPEs. One important requirement for successful *I*−*V* measurement is that the test molecules are able to form an ordered and dense monolayer on a metal substrate. Therefore, prior to the measurements, all self-assembled monolayers (SAMs) were characterized by cyclic voltammogram (CV) and X-ray photoelectron spectroscopy (XPS) to determine basic properties such as coverage and film thickness.

Figure 1a shows the redox current change after the Au electrode was immersed in solution of OPE5 for 2, 10, 40, 120, 360, 1080, or 2880 min. The growth rate of SAM of OPE5 on a Au electrode is presented in Figure 1b. The coverage (θ) of the SAM-modified Au electrode was defined as $\theta(t) = 1 - I_t/I_0$, where $\theta(t)$ was the surface coverage as a function of time, and I_0 and I_t were

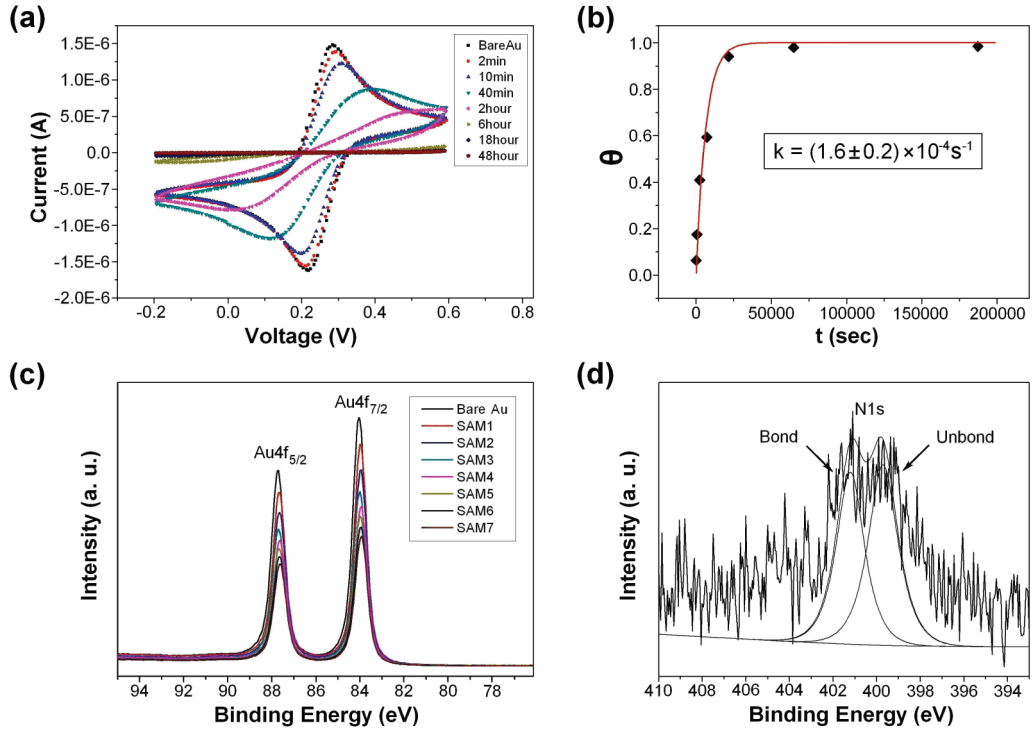

Figure 1. (a) CV curves of $KCl/K_3[Fe(CN)_6]$ (0.5 M/5 mM) on Au electrodes before (■) and after being immersed in solution of OPE5 for 2 min (●), 10 min (▲), 40 min (▼), 120 min (solid left triangle), 360 min (solid right triangle), 1080 min (♦) and 2880 min (solid pentagon). (b) Growth rate of the SAM of OPE5 on a Au electrode. (c) XPS spectra of Au4f region for bare Au electrode and SAMs of OPE1−OPE7 modified Au electrode. (d) XPS spectra of N1S region for the SAM of OPE5 with two distinct peaks.

TABLE 1. Main Parameters of OPE Molecules and Their SAMs

molecule	length (nm)	film thickness (nm)	single molecular resistance (MΩ)	*n* in I,I′ $I \propto V^n$	*n* in II′ $I \propto V^n$	V_{trans} (V)	$V_{II'}$ (V)
OPE1	0.98	0.49	5.623 ± 0.752	1.11		0.59	
OPE2	1.67	0.99	23.32 ± 2.47	1.13		0.64	
OPE3	2.41	1.45	101.0 ± 7.00	1.09		0.65	
OPE4	3.04	1.82	116.3 ± 8.50	1.15	2.11	1.14	0.49
OPE5	3.73	2.08	149.9 ± 11.7	1.02	2.11	1.23	0.53
OPE6	4.43	2.38	184.7 ± 13.7	1.10	2.13	1.12	0.52
OPE7	5.11	2.65	217.3 ± 17.0	1.04	2.18	1.17	0.51

the redox currents of the bare Au electrode in the beginning and the SAM-modified Au electrode at various times, respectively. The entire absorption process followed the Langmuir equation, $\theta = 1 - \exp(-kt)$, where the rate constant k of the adsorption at $(1.6 \pm 0.2) \times 10^{-4}$ s^{-1} was resolved by a nonlinear simulation according to the Langmuir equation.

The thickness of the SAM can be estimated using the attenuation of the Au 4f signal from the substrate (as illustrated in Figure 1c) in XPS measurement according to eq 1:

$$I_{substrate} = I_{SAM} \exp(d/\lambda \sin \theta) \quad (1)$$

where d is the film thickness, $I_{substrate}$ and I_{SAM} are average intensities of Au $4f_{5/2}$ and $4f_{7/2}$ peaks before and after monolayer assembly, respectively, θ is the angle of photoelectron detection, and λ is the effective attenuation length of the photoelectron (4.2 ± 0.1 nm). The seven film thicknesses were calculated and are listed in Table 1. Figure 1d illustrates the XPS scans of the N1s region in SAM of OPE5. Two types of N atoms in the SAM were observed with binding energies of 399.8 and 401.2 eV. Comparing the XPS scans of OPE5 powder, the peak at 399.8 eV was assigned to the nitrogen atoms that were not bonded to the Au substrate, whereas the high-energy peak was related to nitrogen atoms in strong interaction with the Au substrate. This was also true when amine-terminated molecules were anchored on Ag, W, and Fe surfaces. The similar intensity of the two peaks indicated that the amine-terminated OPE molecules adsorbed on the substrate were all standing up, not lying down.

Therefore, on the basis of CV and XPS experiments, a compact and standing up SAM was concluded to have formed after a 48 h assembly, which was very important for the subsequent $I-V$ characterization.

STM Break Junction Measurements for Single Molecular Resistance. The modified STM break junction method used in this paper to measure the single molecule resistance was operated in ambient atmosphere rather than in liquid because SAMs of the amine-terminated oligomers were stable in air for more than 1 week with only 3% resistance fluctuation. The six traces of current *versus* stretching distance for the SAM of OPE3 depicted in Figure 2a show well-defined steps appearing at an integer multiple of *ca.* 0.5 nA. The histogram of currents for 500 break junctions with a 0.05 V tip bias in Figure 2b shows a series of distinct peaks corresponding to one, two, and three molecules between the tip and the Au substrate.

The histogram was fitted with Gaussian distribution to determine the peak centers and full widths at half-height (fwhh), and the peak values were plotted against peak number, as shown in the inset of Figure 2b. The slope was determined by the least-squares fit, with the data points weighted using the fwhh as error bars. The slope revealed the current running through single molecule at this bias, and the same analysis was used for OPE5 (see Figure 2c,d). The plots of current *versus* bias for all seven OPE molecules are shown in Figure 2e. All of these $I-V$ characteristics were linear in the measured range; the single molecular resistance data (listed in Table 1) were conveniently obtained from the slopes of these lines, which were plotted against molecular lengths on a natural log scale (illustrated in Figure 2f).

A clear transition of the length dependence of molecular resistance occurred between OPE3 and OPE4, indicating that the charge transport mechanism dominating in OPE1−OPE3 was different from that in the longer OPE molecules. The linear fit of these short length OPE data points indicated in Figure 2f was well-fitted with the exponential scale equation (eq 2) describing tunneling behavior:

$$R = R_0 \exp(\beta l) \quad (2)$$

where R was the junction resistance, R_0 was the contact resistance, β was the exponential prefactor, and l was the molecular length. The molecular length was calculated by density functional theory approximation using the B3PW91 function coupled with the 6-311G(d,p) basis set plus the N−Au distance. The value of β was 2.02 ± 0.02 nm^{-1}, in close agreement with that obtained for the thiol-terminated OPE molecules by CP-AFM.[20] The value of R_0 was determined as 7.85×10^5 Ω from the y-intercept of the linear fit, which was larger than that of the thiol-terminated system.[5] The effect of terminal groups on tunneling efficiency and contact resistance was consistent with previous reports.[32]

A much smaller slope ($\beta = 0.30$ nm^{-1}) of resistance *versus* length relation was observed for longer

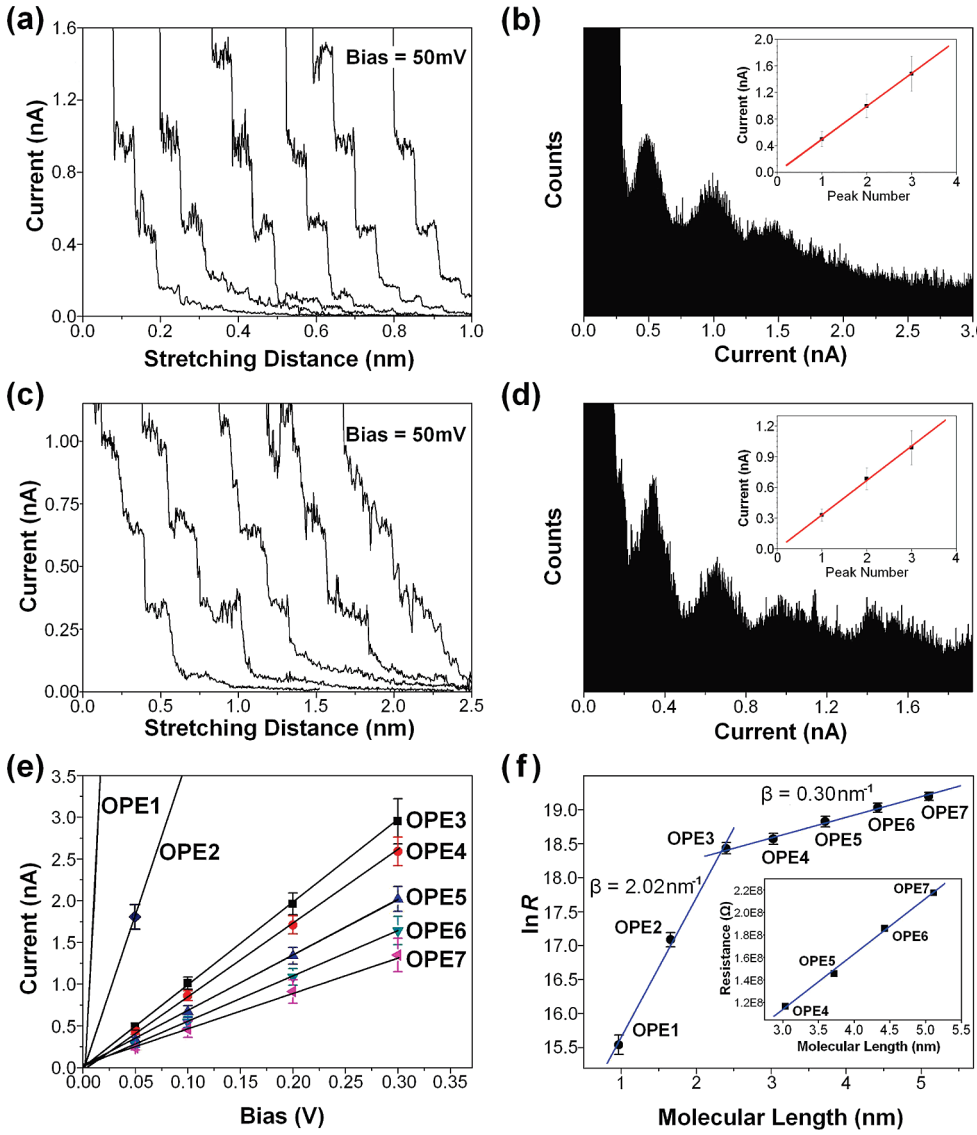

Figure 2. (a) Plots of current *versus* stretching distance for OPE3 at a bias of 50 mV. (b) Histogram of recorded currents with peaks at *ca.* 0.5, 1.0, and 1.5 nA. The slope of peak value *versus* peak number (inset) yields the current per molecule. (c) Plots of currents *versus* stretching distance data for OPE5 at bias of 50 mV. (d) Histogram of recorded currents with peaks at *ca.* 0.33, 0.67, and 1 nA. (e) Current−voltage characteristics for the seven diamine-terminated molecules. The lines are the linear fits, which could yield the most probable single molecular resistance. (f) Semilog plot of single molecular resistance *versus* molecular length for all of the Au−molecular wire−Au junctions. The lines are linear fits according to eq 2. The inset is a linear plot of resistance against length, demonstrating the linear scaling of resistance with length for longer OPE molecules.

OPE molecules, with the extremely small β value indicating that the dominating charge transport mechanism in this regime should be hopping. The plot of molecular resistance *versus* length (Figure 2f, inset) showed a linear characteristic for long OPE molecules, indicating the charge transport mechanism transition from tunneling to hopping was near 2.75 nm.

CP-AFM for *I*−*V* Measurement and Quantum Chemistry Calculation. The semilog plot of *I versus V* for all seven OPE molecules in Figure 3a showed that current decreased with the length increase, which was also observed in Figure 2f. However, a relatively larger current change in all voltage ranges was observed for shorter OPE molecules, while for longer OPE molecules, the same length change resulted a much smaller decrease in current. As can be seen from the plot of log *I versus* electric field *E* (Figure 3a, inset), the charge transport had field-driven characteristics for longer OPE molecules, namely, the *I*−*E* traces collapsed on top of one another. In contrast, there was no collapse for shorter OPE molecules because the tunneling transport was a voltage-driven process. Figure 3b illustrates log *I versus* log *V* characteristics for OPE3 and OPE5, two representatives of short and long molecules, respectively. For OPE3, an obvious transition occurring at 0.65 V existed and the entire transport region was divided into two regimes, labeled as I and II. The situation became more complicated for OPE5, with two inflection points at 0.53 and 1.23 V dividing the transport region into three regimes, labeled I′, II′, and III′. The slope in regime I for OPE3 demonstrated that the current scaled linearly with voltage, which was typical *I*−*V* behavior of tunneling transport in the low-bias regime, according to the Simmons approximation. The Simmons model is a representative quantum mechanical model for tunneling mechanism, as shown in eq 3:

$$I = \frac{Ae}{4\pi^2\hbar d^2}\left\{\left(\phi - \frac{eV}{2}\right)\exp\left(-\frac{2d\sqrt{2m}}{\hbar}\sqrt{\phi - \frac{eV}{2}}\right) - \left(\phi + \frac{eV}{2}\right)\exp\left(-\frac{2d\sqrt{2m}}{\hbar}\right)\sqrt{\phi + \frac{eV}{2}}\right\} \quad (3)$$

where *A* is the junction area, *d* is the molecular length, *m* is the electron effective mass, ϕ is the barrier height, and *e*

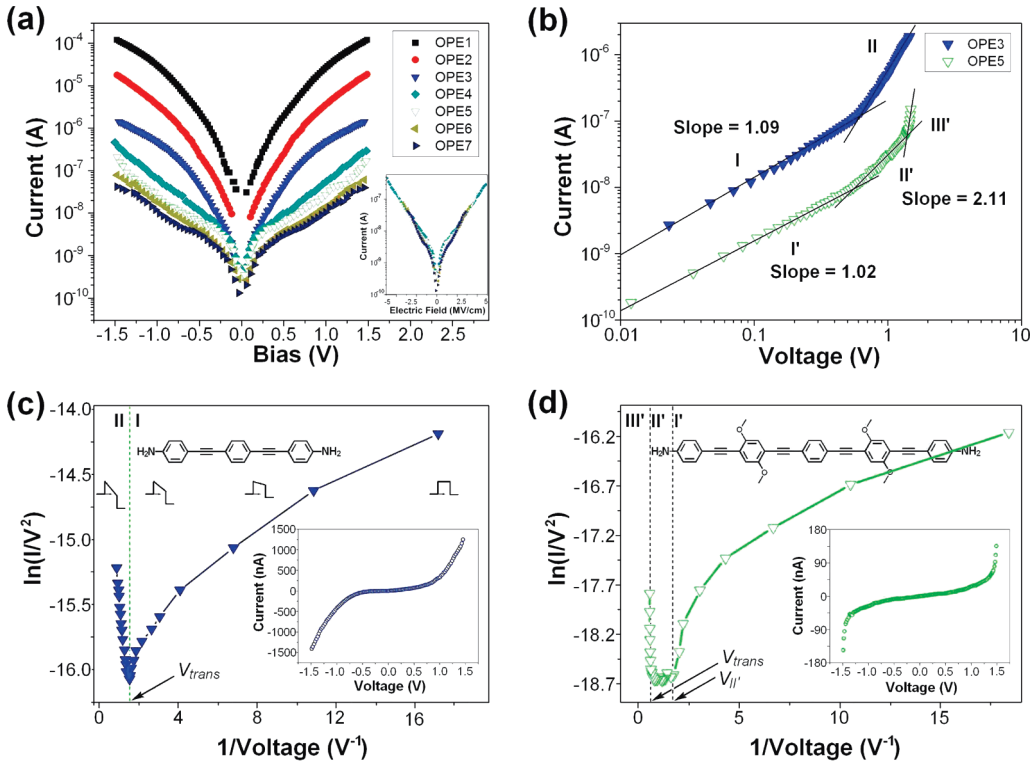

Figure 3. (a) Semilog plot of the average current of 10 *I*−*V* traces for Au−molecular wires−Au junctions. The inset is a semilog plot of current *versus* electric field for longer OPE molecules. (b) Log−log plot of the average of 10 *I*−*V* traces for the Au−OPE3−Au and Au−OPE5−Au junctions, where fits are shown in different transport regimes. (c) Fowler−Nordheim plot for the OPE3 *I*−*V* data (inset), where two distinct regimes are clearly observed. (d) Fowler−Nordheim plot for the OPE5 *I*−*V* data (inset), where three distinct regimes are shown.

is the electronic charge. At low bias, this equation can be reduced approximately to eq 4:

$$I \propto V \exp\left(-\frac{2d\sqrt{2m\phi}}{\hbar}\right) \quad (4)$$

which represents a direct tunneling mechanism with a linear *I*−*V* relation, similar to that in Figure 3b. At the opposite limit, as the bias exceeds the barrier height, the relationship between current and voltage can be described as eq 5:

$$I \propto V^2 \exp\left(-\frac{4d\sqrt{2m\phi^3}}{3\hbar eV}\right) \quad (5)$$

which is also referred to as the field emission mechanism.

In general, to simplify the analysis of *I*−*V* characteristics, eq 5 is transformed to the Fowler−Nordheim relation (eq 6):

$$\ln\left(\frac{I}{V^2}\right) \propto \frac{-4d\sqrt{2m\phi^3}}{3\hbar e}\left(\frac{1}{V}\right) \quad (6)$$

The Fowler−Nordheim plot of OPE3 in Figure 3c revealed that a distinct transition occurred in transport behavior. The transition voltage corresponding to the inflection point in Figure 3b was equal to the low-bias barrier height. All three barrier height values for shorter OPE molecules are listed in Table 1. The change of the current with voltage in the low-bias region is shown in Figure 3b; only the transport property in the high-bias region was analyzed. In regime II, the current scaled linearly with 1/*V*, with a negative slope characteristic of field emission. It should be noted that the logos on the top of Figure 3c are representations of the barrier shapes, which are rectangular, trapezoidal, and triangular from right to left (or from low-bias to high-bias).

Similar analysis was carried out for longer OPE molecules. As can be seen from Figure 3b,d, a new transitional zone appeared in the plot of OPE5 compared with that of OPE3. This was not a simple transition between direct tunneling and field emission because the charge transport mechanism in the low-bias region was different from that in shorter OPE molecules, as indicated by the sharp change in the length dependence of resistance in the STM-BJ experiment. The most reasonable explanation was that, in the low-bias region, the charge transport was dominated by an ohmic hopping mechanism—a field-driven conduction with a linear relationship with voltage. In contrast, in the high-bias region, the field emission was still dominating, as indicated by the negative slope. Frisbie made an in-depth and comprehensive discussion on conduction mechanisms for longer conjugated molecules[22] and suggested that the special zone in regime II′ should receive more attention. However, at this time, few investigations have been carried out related to this zone. To

obtain enough supporting information, a further study in this regime is currently being done by another colleague.

The above results are further supported by quantum chemistry calculations for all of the OPE molecules studied. The charge transport mechanism is known to be influenced by molecular electronic structures, namely, the energy gap between the highest occupied molecular orbital (HOMO) and the lowest unoccupied molecular orbital (LUMO), and the alignment of two frontier molecular orbitals to the metal Fermi level. When the difference in energy between the LUMO and the Fermi level is large, charge transport occurs by tunneling. In contrast, if the Fermi level approaches the LUMO, hopping conduction may take place.[33] Figure 4 shows the calculated electronic structure characteristics of the seven OPE molecules, incorporating the HOMO and LUMO level. The energy gaps (E_g) obtained from quantum chemistry calculations and UV−visible spectroscopy were also given, which were very close to each other, indicating the suitability of theoretical simulation. For all of the OPE molecules studied, the HOMO levels showed only small fluctuations, while the LUMO level decreased significantly from OPE1 to OPE4. This indicated that the OPE molecules with more than three repeating units could be the potential channels for hopping conduction.

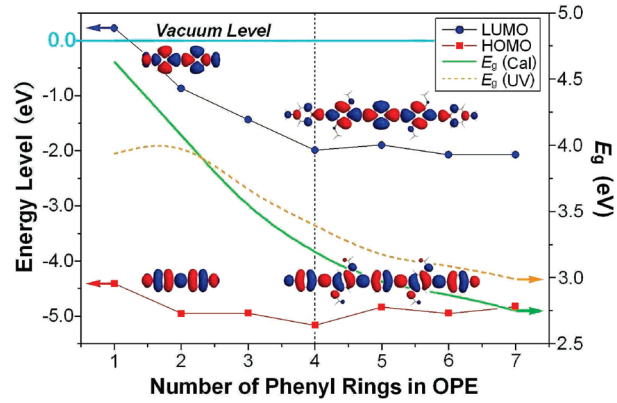

Figure 4. Illustration of the HOMO, LUMO, and E_g of OPE1−OPE7 obtained from UV−visible spectroscopy and quantum chemistry calculation.

SUMMARY

A comprehensive investigation has been made on charge transport characteristics of OPE molecules, using modified STM break junction and CP-AFM methods in combination with a quantum chemistry calculations. The charge transport mechanism experienced an intrinsic transition from tunneling to hopping near 2.75 nm. In addition, theoretical calculation provided an essential explanation for these phenomena in light of molecular electronic structures. Currently, the synthesis and measurements for much longer OPE molecules and ferrocene-based OPE molecules are ongoing in our laboratory.

MATERIALS AND METHODS

Materials. Tetrahydrofuran (THF) was distilled under nitrogen over sodium benzophenone ketyl. Other reagents and solvents were purchased from commercial suppliers and used without further purification. The synthesis of the molecular wires in Scheme 1 is described in Supporting Information.

Preparation of the Conjugated Molecular Wire SAMs. The target conjugated molecular wire (50 μM) was dissolved in 10 mL of THF under nitrogen atmosphere. After the Au substrate was immersed in the solution for 48 h in the absence of the light, it was rinsed with dry THF ultrasonically and dried under a nitrogen stream to give conjugated molecular wire SAMs.

Cyclic Voltammogram Measurements. All of the CV curves were recorded on Solartron SI 1287 electrochemical interface using a conventional three-electrode cell comprising a Au work electrode, a platinum flag counter electrode, and a Ag/AgCl reference electrode. A 5.0 mM $K_3Fe(CN)_6/K_4Fe(CN)_6$ solution with 0.5 M KCl as supporting electrolyte was prepared freshly prior to use. Under nitrogen protection, one of the OPE molecules was dissolved in a mixture solvent of ethanol/CH_2Cl_2 (95:5, v/v) to make a concentration of 0.5 mM. A clean Au electrode was then immersed into the solution in the absence of light. The SAM was formed on the Au surface *via* the amine−Au link chemistry, and then the SAM-modified Au electrode was rinsed with ethanol ultrasonically and dried under nitrogen stream for a measurement.

XPS Measurements. The XPS spectra of SAMs on Au substrates after 48 h immersion were carried out on a VG Scientific ESCALAB 250 spectrometer with Al Kα X-ray source (1486.5 eV) using a pass energy of 20 eV at takeoff angles of 90°. Surface charge effect was compensated by referencing the adventitious C1s peak at 284.6 eV.

Single Molecular Resistance by STM Break Junctions. STM break junctions were operated under ambient atmosphere using Au STM tips, following a modified procedure of Xu and Tao.[34−41] Gold tips could penetrate into the SAM at −50 or −100 mV with current set-point in the range of 0.5−10 nA, and the N−Au bond was therefore formed. The feedback was then disabled, and the tip was lifted at a vertical rate of 4 nm/s while keeping the *X*−*Y* position constant. The current was recorded as a function of the traveling distance when the tip with a fixed bias was repeatedly pushed into and retracted from the substrate to form and break the molecule junctions. This procedure was repeated thousands of times for each sample, and statistical analysis was constructed to extract single molecular resistance from the staircase-like current−distance (*I*−*S*) curves.

CP-AFM Experiments. The CP-AFM experiments were performed at room temperature under ambient atmosphere on a Digital Instruments (Santa Barbara, CA) Nanoscope IIIA Multimode equipped with an E-scanner and current sensitive attachment. Contact mode silicon cantilevers coated with Au (MikroMasch) were used. Au conductive tip was in contact with SAMs as the top electrode, and the Au substrate served as the bottom electrode. Each *I*−*V* curve was recorded at an applied load of 2 nN using the same tip; *I*−*V* curves were collected at five different places for each SAM, and 5−10 measurements were conducted at each place.

Ultraviolet−Visible Spectroscopy. The ultraviolet−visible (UV−vis) absorption spectra were recorded from a Varian 50 Bio spectrom-

eter at room temperature in THF with conventional 1.0 cm quartz cells.

Quantum Chemistry Computation. The estimated length and electronic structures of the molecular wires were calculated by density functional theory approximation, using the B3PW91 function coupled with the 6-311G(d,p) basis set.

Acknowledgment. This work was supported by the Natural Science Foundation of China (Grant No. 20225414). We gratefully thank editor and reviewers for the insightful and helpful comments.

Supporting Information Available: Experimental details for the synthesis of all the OPE molecules; ^{1}H, ^{13}C, and MS spectra; UV−visible spectra; quantum chemistry calculation. This material is available free of charge *via* the Internet at http://pubs.acs.org.

REFERENCES AND NOTES

1. Bumm, L. A.; Arnold, J. J.; Cygan, M. T.; Dunbar, T. D.; Burgin, T. P.; Jones, L., II; Allara, D. L.; Tour, J. M.; Weiss, P. S. Are Single Molecular Wires Conducting? *Science* **1996**, *271*, 1705–1707.
2. Chem, J.; Reed, M. A.; Rawlett, A. M.; Tour, J. M. Large On−Off Ratios and Negative Differential Resistance in a Molecular Electronic Device. *Science* **1999**, *286*, 1550–1552.
3. Tour, J. M.; Reed, M. A.; Seminario, J. M.; Allara, D. L.; Weiss, P. S. Molecular Computer. United States Patent US 6,430,511 B1.
4. Beebe, J. M.; Kim, B.; Gadzuk, J. W.; Frisbie, C. D.; Kushmerick, J. G. Transition from Direct Tunneling to Field Emission in Metal−Molecule−Metal Junctions. *Phys. Rev. Lett.* **2006**, *97*, 026801.
5. Wold, D. J.; Haag, R.; Rampi, M. A.; Frisbie, C. D. Distance Dependence of Electron Tunneling through Self-Assembled Monolayers Measured by Conducting Probe Atomic Force Microscopy: Unsaturated *versus* Saturated Molecular Junctions. *J. Phys. Chem. B* **2002**, *106*, 2813–2816.
6. Nakamura, T.; Fujitsuka, M.; Araki, Y.; Ito, O.; Ikemoto, J.; Takimiya, K.; Aso, Y.; Otsubo, T. Photoinduced Electron Transfer in Porphyrin-Oligothiophene-Fullerene Linked Triads by Excitation of a Porphyrin Moiety. *J. Phys. Chem. B* **2004**, *108*, 10700–10710.
7. Weiss, E. A.; Ahrens, M. J.; Sinks, L. E.; Gusev, A. V.; Ranter, M. A.; Wasielewski, M. R. Making a Molecular Wire: Charge and Spin Transport through *para*-Phenylene Oligomers. *J. Am. Chem. Soc.* **2004**, *126*, 5577–5584.
8. Shimazaki, T.; Asai, Y.; Yamashita, K. Theoretical Rate Constants of Super-Exchange Hole Transfer and Thermally Induced Hopping in DNA. *J. Phys. Chem. B* **2005**, *109*, 1295–1303.
9. Welter, S.; Lafolet, F.; Cecchetto, E.; Vergeer, F.; Cola, L. D. Energy Transfer by a Hopping Mechanism in Dinuclear Ir^{III}/Ru^{II} Complexes: A Molecular Wire. *ChemPhysChem* **2005**, *6*, 2417–2427.
10. Reed, M. A.; Zhou, C.; Muller, C. J.; Burgin, T. P.; Tour, J. M. Conductance of a Molecular Junction. *Science* **1997**, *278*, 252–254.
11. Salomon, A.; Cahen, D.; Lindsay, S.; Tomfohr, J.; Engelkes, V. B.; Frisbie, C. D. Comparison of Electronic Transport Measurements on Organic Molecules. *Adv. Mater.* **2003**, *15*, 1881–1890.
12. Kim, B.; Beebe, J. M.; Olivier, C.; Rigaut, S.; Touchard, D.; Kushmerick, J. G.; Zhu, X. Y.; Frisbie, C. D. Temperature and Length Dependence of Charge Transport in Redox-Active Molecular Wires Incorporating Ruthenium(II) Bis(δ-arylacetylide) Complexes. *J. Phys. Chem. C* **2007**, *111*, 7521–7526.
13. Holmlin, R. E.; Haag, R.; Chabinyc, M. L.; Ismagilov, R. F.; Cohen, A. E.; Terfort, A.; Rampi, M. A.; Whitesides, G. M. Electron Transport through Thin Organic Films in Metal−Insulator−Metal Junctions Based on Self-Assembled Monolayers. *J. Am. Chem. Soc.* **2001**, *123*, 5075–5085.
14. Lewis, P. A.; Inman, C. E.; Yao, Y.; Tour, J. M.; Hutchison, J. E.; Weiss, P. S. Mediating Stochastic Switching of Single Molecules Using Chemical Functionality. *J. Am. Chem. Soc.* **2004**, *126*, 12214–12215.
15. Sedghi, G.; Sawada, K.; Esdaile, L. J.; Hoffmann, M.; Anderson, H. L.; Bethell, D.; Haiss, W.; Higgins, S. J.; Nichols, R. J. Single Molecule Conductance of Porphyrin Wires with Ultralow Attenuation. *J. Am. Chem. Soc.* **2008**, *130*, 8582–8583.
16. Moore, A. M.; Mantooth, B. A.; Donhauser, Z. J.; Maya, F.; Price, D. W.; Yao, Y.; Tour, J. M.; Weiss, P. S. Cross-Step Place-Exchange of Oligo(phenylene-ethynylene) Molecules. *Nano. Lett.* **2005**, *5*, 2292–2297.
17. Liu, K.; Wang, X.; Wang, F. Probing Charge Transport of Ruthenium-Complex-Based Molecular Wires at the Single-Molecule Level. *ACS Nano* **2008**, *2*, 2315–2323.
18. Weiss, P. S. Functional Molecules and Assemblies in Controlled Environments: Formation and Measurements. *Acc. Chem. Res.* **2008**, *41*, 1772–1781.
19. Beebe, J. M.; Kim, B.; Frisbie, C. D.; Kushmerick, J. G. Measuring Relative Barrier Heights in Molecular Electronic Junctions with Transition Voltage Spectroscopy. *ACS Nano* **2008**, *2*, 827–832.
20. Liu, K.; Li, G.; Wang, X.; Wang, F. Length Dependence of Electron Conduction for Oligo(1,4-phenylene ethynylene)s: A Conductive Probe-Atomic Force Microscopy Investigation. *J. Phys. Chem. C* **2008**, *112*, 4342–4349.
21. Kim, B.; Beebe, J. M.; Jun, Y.; Zhu, X. Y.; Frisbie, C. D. Correlation between HOMO Alignment and Contact Resistance in Molecular Junctions: Aromatic Thiols *versus* Aromatic Isocyanides. *J. Am. Chem. Soc.* **2006**, *128*, 2970–2971.
22. Choi, S. H.; Kim, B.; Frisbie, C. D. Electrical Resistance of Long Conjugated Molecular Wires. *Science* **2008**, *320*, 1482–1486.
23. Shirai, Y.; Sasaki, T.; Guerrero, J. M.; Yu, B. C.; Hodge, P.; Tour, J. M. Synthesis and Photoisomerization of Fullerene- and Oligo(phenylene ethynylene)-Azobenzene Derivatives. *ACS Nano* **2008**, *2*, 97–106.
24. Moore, A. M.; Dameron, A. A.; Mantooth, B. A.; Smith, R. K.; Fuchs, D. J.; Ciszek, J. W.; Maya, F.; Yao, Y.; Tour, J. M.; Weiss, P. S. Molecular Engineering and Measurements To Test Hypothesized Mechanisms in Single Molecule Conductance Switching. *J. Am. Chem. Soc.* **2006**, *128*, 1959–1967.
25. Ashwell, G. J.; Urasinska, B.; Wang, C.; Bryce, M. R.; Grace, I.; Lambert, C. J. Single-Molecule Electrical Studies on a 7nm Long Molecular Wire. *Chem. Commun.* **2006**, 4706–4708.
26. Guisinger, N. P.; Greene, M. E.; Basu, R.; Baluch, A. S.; Hersam, M. C. Room Temperature Negative Differential Resistance through Individual Organic Molecules on Silicon Surfaces. *Nano. Lett.* **2004**, *4*, 55–59.
27. He, J.; Fu, Q.; Lindsay, S.; Ciszek, J. W.; Tour, J. M. Electrochemical Origin of Voltage-Controlled Molecular Conductance Switching. *J. Am. Chem. Soc.* **2006**, *128*, 14828–14835.
28. Kumar, A. S.; Ye, T.; Takami, T.; Yu, B. C.; Flatt, A. K.; Tour, J. M.; Weiss, P. S. Reversible Photo-Switching of Single Azobenzene Molecules in Controlled Nanoscale Environments. *Nano. Lett.* **2008**, *8*, 1644–1648.
29. Risko, C.; Zangmeister, C. D.; Yao, Y.; Marks, T. J.; Tour, J. M.; Ranter, M. A.; Zee, R. D. Experimental and Theoretical Identification of Valence Energy Levels and Interface Dipole Trends for a Family of (Oligo)phenylene-ethynylenethiols Adsorbed on Gold. *J. Phys. Chem. C* **2008**, *112*, 13215–13225.
30. Venkataraman, L.; Klare, J. E.; Tam, I. W.; Nuckolls, C.; Hybertsen, M. S.; Steigerwald, M. L. Single-Molecule Circuits with Well-Defined Molecular Conductance. *Nano. Lett.* **2006**, *6*, 458–462.
31. Huber, R.; Gonzalez, M. T.; Wu, S.; Langer, M.; Grunder, S.; Horhoiu, V.; Mayor, M.; Bryce, M. R.; Wang, C.; Jitchati, R.; et al. Electrical Conductance of Conjugated Oligomers at the Single Molecule Level. *J. Am. Chem. Soc.* **2008**, *130*, 1080–1084.

32. Chen, F.; Li, X.; Hihath, J.; Huang, Z.; Tao, N. Effect of Anchoring Groups on Single-Molecule Conductance: Comparative Study of Thiol-, Amine-, and Carboxylic-Acid-Terminated Molecules. *J. Am. Chem. Soc.* **2006**, *128*, 15874–15881.
33. Weiss, E. A.; Wasielewski, M. R.; Ranter, M. A. Molecular as Wires: Molecule-Assisted Movement of Charge and Energy. *Top. Curr. Chem.* **2005**, *257*, 103–133.
34. Xu, B.; Tao, N. J. Measurement of Single-Molecule Resistance by Repeated Formation of Molecular Junctions. *Science* **2003**, *301*, 1221–1223.
35. He, J.; Sankey, O.; Lee, M.; Tao, N.; Li, X.; Lindsay, S. Measuring Single Molecule Conductance with Break Junctions. *Faraday Discuss.* **2006**, *131*, 145–154.
36. Venkataraman, L.; Park, Y. S.; Whalley, A. C.; Nuckolls, C.; Hybertsen, M. S.; Steigerwald, M. L. Electronics and Chemistry: Varying Single-Molecule Junction Conductance Using Chemical Substituents. *Nano. Lett.* **2007**, *7*, 502–506.
37. Lindsay, S. M.; Ranter, M. A. Molecular Transport Junctions: Clearing Mists. *Adv. Mater.* **2007**, *19*, 23–31.
38. Quinn, J. R.; Foss, F. W.; Venkataraman, L.; Hybertsen, M. S.; Breslow, R. Single-Molecule Junction Conductance through Diaminoacenes. *J. Am. Chem. Soc.* **2007**, *129*, 6714–6715.
39. He, J.; Chen, F.; Li, J.; Sankey, O. F.; Terazono, Y.; Herrero, C.; Gust, D.; Moore, T. A.; Moore, A. L.; Lindsay, S. M. Electronic Decay Constant of Carotenoid Polyenes from Single-Molecule Measurements. *J. Am. Chem. Soc.* **2005**, *127*, 1384–1385.
40. Park, Y. S.; Widawsky, J. R.; Kamenetska, M.; Steigerwald, M. L.; Hybertsen, M. S.; Nuckolls, C.; Venkataraman, L. Frustrated Rotations in Single-Molecule Junctions. *J. Am. Chem. Soc.* **2009**, *131*, 10820–10821.
41. Xu, B. Q.; Li, X. L.; Xiao, X. Y.; Sakaguchi, H.; Tao, N. J. Electromechanical and Conductance Switching Properties of Single Oligothiophene Molecules. *Nano. Lett.* **2005**, *5*, 1491–1495.